AIChE

Influence of the Boundary Conditions on Capillary Flow Dynamics and Liquid Distribution in a Porous Medium

B. Markicevic, H. Li, A. R. Zand, and H. K. Navaz
Dept. of Mechanical Engineering, Kettering University, Flint, MI 48504

DOI 10.1002/aic.12788
Published online November 7, 2011 in Wiley Online Library (wileyonlinelibrary.com).

After depositing a wetting liquid onto a porous medium surface, and under the influence of the capillary pressure, the liquid is imbibed into the porous medium creating a wetted imprint. The flow within the porous medium does not cease once all the liquid is imbibed but continues as a secondary capillary flow, where the liquid flows from large pores into small pores along the liquid interface. The flow is solved using the capillary network model, and the influence of the boundary condition on the liquid distribution within the porous medium is investigated. The pores at the porous medium boundaries can be defined as open or closed pores, where an open pore is checked for the potential threshold condition for flow to take place. In contrast, the closed pore is defined as a static entity, in which the potential condition for flow to take place is never satisfied. By defining the pores at distinct porous medium boundaries as open or closed, one is able to obtain a very different liquid distribution within the porous medium. The liquid saturation profiles along the principal flow direction, ranging from constant to steadily decreasing, to the profile with a local maximum, are found numerically. It is shown that these saturation profiles are also related to the geometrical dimension that is perpendicular to the flow principal direction, and changing the boundary type from open to closed allows the liquid distribution within the porous medium to be controlled. In addition to the liquid distribution, the influence of the boundary conditions on capillary pressure and relative permeability is investigated, where both parameters are not influenced by variation of the boundary condition types. © 2011 American Institute of Chemical Engineers *AIChE J,* 58: 2911–2919, 2012
Keywords: porous media, interfacial processes, fluid mechanics

Introduction

The secondary capillary flows, which are defined as internal liquid flows within porous medium after the liquid from the porous medium surface is completely imbibed by porous medium, are not addressed comprehensively regardless of the fact that these flows are often present. Some typical cases include underground water flows,[1] drying, oil recovery,[2] printing,[3] or even everyday problems as in diapers. In common to all of these applications is that the imbibed volume of liquid spreads further in the porous medium until an equilibrium liquid phase distribution in the porous medium is reached. Clearly, the secondary capillary flows are multiphase flows, where a constant volume (initially imbibed) spreads into previously dry regions of porous medium.[4] Furthermore, they are purely driven by the capillary force at the wetted/dry interface within porous medium, as the capillary flow is caused by porous medium heterogeneity,[5] and the liquid flows locally at the interface from the points of higher potential to the points of lower potential. Due to the secondary capillary flows, the liquid distribution within the porous medium changes. Over time, highly saturated regions become less saturated, and at the same time, previously dry regions become wet to some extent, altering the spatial "wetness" within the porous medium; the effect used in diapers. Similarly, in oil recovery, one can investigate how the remaining oil is redistributed in the well, looking for the strategies on how to promote the agglomeration of the remaining oil phase (due to the enhanced secondary flow of another phase).

The existence of the secondary capillary flow is observed both experimentally and numerically in the sessile droplet simultaneous secondary spread and evaporation problem (see, e.g., Markicevic and Navaz[6] and references therein). It has been shown that the increase of the wetted volume in the porous medium can be significant, with the saturation decreasing for an order of magnitude before the equilibrium liquid distribution is reached.[7] Similarly, in the drying problem, the initial mass loss is linear in time and this constant drying rate can be prolonged due to the secondary flow, which replenishes the liquid closer to the evaporation boundary. For evaporation from semi-infinite domains, the secondary flow is also responsible for "tail" in the evaporation curve as liquid protrudes deeper into porous medium compared to the case without the secondary flow, and, therefore, it takes longer for the liquid to evaporate. Hence, four distinct regions can be defined in the secondary flow or evaporation problem, where, between fully saturated and dry regions of porous medium, a partially saturated region exists in which the liquid content (saturation) changes from zero to one.[8–11]

Correspondence concerning this article should be addressed to H. K. Navaz at hnavaz@kettering.edu.

The liquid distribution within the partially saturated region is not the same in low and highly saturated subregions. For the liquid low saturation both the less-branched carrying backbones and liquid ganglia (insulated parts of liquid phase) are present, whereas the highly saturated subregion consists mainly of a single branched carrying backbone in which the liquid phase is connected continuously. Finally, for longer times, and due to the secondary capillary flow (or evaporation), the fully saturated region fades, becoming a partially saturated region with the capillary flow rate decreasing before the liquid distribution reaches an equilibrium,[7] or becomes equal to zero due to the evaporation.[6]

The capillary network models, in which an actual porous medium is represented as a network of volumetric elements—pores connected by transport resistance elements—throats can be used to solve the secondary flow problem.[12] For a specific processes such as a slow drainage, the formulation which utilizes a specific mechanistic rule, as in invasion percolation[13] can be used. However, for the general solution in which the capillary number changes in time, the dynamic formulation based on the potential at the interface needs to be implemented.[4,14,15] In the secondary flow, in addition to the change of the capillary number, there is a change of the flow mechanism. Initially, the gas-liquid interface is located close to the fully saturated region, and one observes in-parallel the local capillary flows at the interface and the viscous flow from the highly saturated region to the low-saturated region. The local flows at the interface are caused from the local differences in the capillary pressure where two adjacent pores or two pores, which are close to each other, have distinct capillary pressures. The length-scale of the flow is equal to a small multiple of throat size. On the other hand, for each larger entity, such as the surface of the highly saturated region or pores which are located at the surface between wetted and non-wetted regions, an average capillary pressure can be defined and there is a viscous flow between two entities. The viscous flow length-scale is equal to the distance between two entities. As the secondary flow progresses, the larger entities for which the specific capillary pressure can be defined gradually vanish, and the secondary capillary flow becomes more of a local phenomenon. Macroscopically, this transition is referred to as the changes in flow type, where the viscous flows are more in the carrying backbone, and the local capillary flows can be seen as a hopping flow between the neighboring pores affecting flow stability.[16–19]

The pores at the gas||liquid interface can be either volumetric, located deeper in the porous medium (e.g., displacing interface), or surface, located at a porous medium boundary. Regardless of their location, the interfacial pores are partially or fully saturated, where the fully saturated pore is formed after emptying an adjacent partially filled pore in the previous discrete step. To obtain a well-imposed problem, the boundary conditions for the secondary capillary flow need to be defined; each pore at the gas||liquid interface has to be checked with respect to the capillary pressure threshold, and, hence, the flow rate in each pore is calculated. It should be noted here that fully saturated volumetric and surface pores differ; all adjacent pores can be full for a surface pore, while at least one adjacent pore is empty for a volumetric pore. Thus, along porous medium boundaries, the question is should the full pores be checked for the capillary pressure threshold, or simply be considered as flow pores, which belong to the fully saturated body of liquid. Furthermore, the wetted boundaries of the porous medium are not all the same, and they can be located next to the solid wall, being the boundary from where the liquid is initially imbibed (inlet) or simply the boundary that is located next to the ambient air. These differences in the porous medium boundaries further complicate the question of how to define the full pores, where on each of these porous medium boundaries, the full pores can have distinct behavior. Finally, the difference in these boundary pores will cause variations in the liquid distribution, where of special interest is whether the relative permeability and capillary pressure remain invariant for the distinct boundary conditions.

Problem Formulation

In the primary imbibitions, the wetting liquid is imbibed by porous medium. Having imbibed a volume of the wetting liquid (V_0) which is less than the overall void volume of the porous medium (V_{void}), wetted and dry volumes of the porous medium can be distinguished. This flow is also referred to as primary spread,[20] and it is shown in Figure 1, where a porous medium rectangular domain is partially wetted by the liquid with the interface (S_{int}) between wet and dry regions (S_{pri}) (note $S_{int} \equiv S_{pri}$). During the primary spread, the liquid flows into the porous medium across an inlet boundary (S_{inl}) with the flow rate greater than zero ($q_b > 0$), and the wetted volume (V_{wet}) is located between S_{inl} and S_{pri}. The secondary capillary flow[4] is defined as a purely capillary flow of the liquid that is already within the porous medium, and without any liquid flow across porous medium boundaries ($q_b = 0$) as shown in Figure 1. The additional wetting of a previously dry porous medium occurs at the expense of depleting the liquid from the wetted volume, and the secondary flow interface (S_{int}) between dry and wet regions (S_{sec}) can be identified as $S_{int} \equiv S_{sec}$. Viewing a porous medium as the network of pores of different sizes, and, due to the varying pore size and corresponding capillary pressures, the smallest pores within the dry volume are filled by liquid from the largest pores located in the wetted region during the secondary flow. Thus, the wetted volume consists of drainage and imbibition regions. Their positions can be approximately defined with respect to S_{pri}, where wetted volume in the primary spread (from S_{inl} to S_{pri}) is partially drained with the liquid filling the pores that belong to the region between S_{pri} and S_{sec}. The interface between the wetted and dry region (S_{sec}) changes in time, and so does wetted volume (V_{wet}). Thus, the secondary flow is exclusively the multiphase flow, as over time, a constant volume of liquid (V_0) wets a larger volume of porous medium (V_{wet}), causing the saturation in the wetted volume of porous medium to decrease, $s = V_0/(\phi V_{wet})$. Finally, the secondary flow is terminated once the equilibrium liquid distribution within porous medium is achieved.

Throughout the secondary flow, the wetted volume of the porous medium (V_{wet}) is bounded by interface between wetted and dry regions (S_{sec}), and by wetted boundaries of the porous medium. As shown in Figure 1, a few distinct boundaries can be identified. All pores within the porous medium volume at liquid interface S_{int} are checked for the capillary pressure boundary condition. The inlet boundary (S_{inl}) is completely immersed in the liquid before the liquid is imbibed by porous medium. The wall boundaries (S_{wall}) are defined as boundaries that are in direct contact with the solid

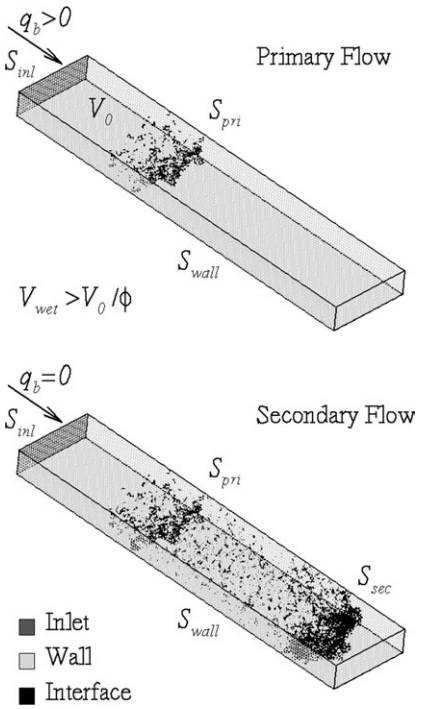

Figure 1. Primary and secondary capillary flow, gas|liquid interfaces and different types of porous medium boundaries wetted by liquid phase.

surface or the ambient air. It is obvious that the behavior of the liquid may differ at all these boundaries, which need to be defined by pertinent boundary conditions. The pores at the porous medium boundary can be viewed as pores for which the capillary pressure threshold boundary condition applies, or simply be considered as flow pores not checked for the capillary pressure. If the boundary pores are set as flow pores, they can be emptied only once they are next to an empty volumetric pore and the capillary pressure condition is satisfied. Therefore, two types of boundary pores can be defined; namely *open* and *closed* pores, the first being checked for the capillary pressure threshold condition and the latter being considered as the flow pores (the net flow in the flow pore is equal to zero). The definition of open and closed pores is shown in Figure 2, with the dashed line representing the porous medium boundary; open pores can undergo the change of being empty or being full an arbitrary number of times during the secondary flow duration.

The dynamics of the secondary flow is governed by instantaneous pressure changes, where from the pressure solution; the flow rates into the open pores at the wetted boundaries of porous medium are computed. For each open pore at the wetted boundaries, and all volumetric pores within porous medium at the interface between gas and liquid phase, two pressures are defined $p_{\text{int}|Gas}$ and $p_{\text{int}|Liq}$. The absolute value of the pressure difference $|p_{\text{int}|Gas} - p_{\text{int}|Liq}|$ compared to the capillary pressure (p_c) threshold gives the condition for the interface to deform

$$\left|p_{\text{int}|Gas} - p_{\text{int}|Liq}\right| \begin{cases} > p_c, \text{ flow} \\ < p_c, \text{ static} \end{cases} \quad (1)$$

where the flow rate into or out of the interfacial pore can take place. For the static pores, the capillary pressure threshold condition is not satisfied and the capillarity keeps the liquid in such a pore. It has been already explained that in the next step, due to the changes of the liquid distribution and liquid pressure, the static pore can have the flow rate different than zero. Due to the heterogeneity of the porous medium, the flow at the interface can be stable or unstable with the interface smoothly advancing or retreating (piston flow and snap-off), or for the flow in one pore which is not similar to the flows in the neighboring pores, gas clusters and liquid ganglia emerge promoting the flow instability. Macroscopically, sudden local changes in flow velocity deform the interface shape which becomes the interface with a finite thickness or the flow front that can lead further to the significant local protrusion of one phase into another referred to as phase fingering. Finally, the flow stability can be altered due to the simultaneous filling and emptying of pores during the secondary capillary flow.

To solve the primary and secondary flow, which accounts for the local flows at the interface governed by the capillary pressure condition in Eq. 1, the capillary network model with the dynamic boundary condition can be used. In the model, the porous medium is replaced by a network consisting of the volume elements—pores and the flow resistive elements—throats. Throughout the spread, the liquid phase pressure is repeatedly solved over the network from the conservation equations (mass and momentum), where the discrete time steps is defined as the minimum time needed for a pore from the interface to become full or empty. After each time step, the new position of the interface is identified. From the calculated pressure, the local flows in each pore at the interface are found, where for each pore at the interface, the flow rate can be positive or negative depending on the local force balance. However, in the next step, the flow direction in each of the pores can be reverted depending on the new pressure solution. For each pore (i) at the interface, the pore saturations at the gas|liquid interface satisfy the $0 < s_{p,i} < 1$ condition, with the pore flow rate greater or smaller

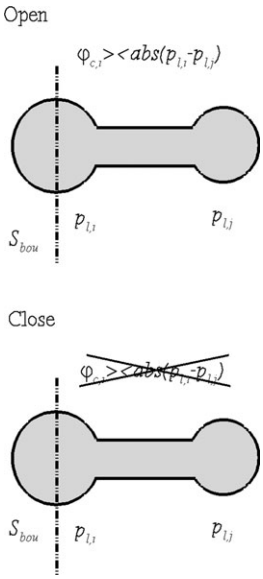

Figure 2. Definition of open and closed pores at the porous medium boundaries (S_{bou}), where the potential condition is used for open pores, and closed pores are set as flow pores in which the potential condition is never satisfied.

than zero, $q_{p,il+}$ and $q_{p,il-}$. Based on the pore flow rate sign, the pore capillary pressure is also defined as $p_{c,p,il+}$ and $p_{c,p,il-}$. Having the flow rates defined, the flow stability is directly accounted for, where the piston flow and snap off are attributed with smaller variations in $q_{p,il+}$ and $q_{p,il-}$. On the other hand, due to the porous medium heterogeneity, the liquid phase can protrude further into the dry part of the porous medium or the gas phase can be entrapped by the liquid phase forming liquid ganglia and gas clusters, respectively. The sizes of both clusters and ganglia are a measure of the flow instability, which is influenced by local variation in $q_{p,il+}$ and $q_{p,il-}$. Finally, to obtain the macroscopic parameters for stable flows, the pore quantities need to be averaged.

Two distinct pressure gradients within the liquid phase can be distinguished intuitively in the secondary capillary flow. Initially, the liquid is distributed in the smaller volume of the porous medium (V_{wet}), has high saturation, and is transported into newly wetted volume. Both of these entities (wetted volume and newly wetted volume) have well defined capillary pressures, and their difference is significant. Due to the difference of the capillary pressures for these two entities, the liquid flow takes place along the length scale equal to the distance between two entities (l_{gl}). Thus, the viscous flow rate is defined

$$q_{vis} \propto -\frac{2\sigma\cos(\theta)}{l_{gl}}\left(\frac{p_{c,pri}}{2\sigma\cos(\theta)}-\frac{1}{r_{p,\mathrm{sec}}}\right) \tag{2}$$

where σ is the liquid surface tension, and θ is the contact angle inside the porous medium. The value of $p_{c,pri}$ is an average capillary pressure in the porous medium volume wetted in the primary spread (located between S_{inl} and S_{pri}), and $r_{p,sec}$ is an average pore radius in the region wetted during the secondary spread (from S_{pri} to S_{sec}). The value of q_{vis} decreases in time as l_{gl} and $p_{c,pri}$ increase (thus, $p_{c,pri}$ approaches $2\sigma\cos(\theta)/r_{p,sec}$). In parallel with the viscous flow, the capillary flow in the partially wetted part of porous medium takes place, where for two pores (i) and (j) close to each other, the capillary flow rate can be expressed as follows

$$q_{cap} \propto \frac{2\sigma\cos(\theta)}{l_{loc}}\left(\frac{1}{r_{p,i}}-\frac{1}{r_{p,j}}\right) \tag{3}$$

As can be seen, the capillary flow rate is proportional to the capillary pressure difference between two pores having pore radii $r_{p,i}$ and $r_{p,j}$. and inversely proportional to the distance between two pores (l_{loc}). Two pores can be next to each other or at a distance equal to a few multiples of distance between the adjacent pores. The capillary flow rate also decreases during the secondary flow, where l_{loc} increases and $1/r_{p,i}-1/r_{p,j}$ decreases in time. Comparing q_{vis} and q_{cap}, it can be seen that q_{vis} is responsible for flow in large entities, whereas q_{cap} gives the magnitude of local flows with both flows occurring at different length scales. Changing the boundary conditions by setting the boundary pores as open or closed, one can change the significance of either of the two flows. Thus, having all pores at the liquid boundaries defined as closed, except for volumetric pores inside the porous medium that are always defined as open, the flow is localized at those pores, and therefore, capillary flow is dominant. If the inlet boundary is defined as consisting of open pores, the viscous flow between the inlet boundary and volumetric pores within porous medium takes place, with the viscous flow direction and additional capillary flow (inlet) coinciding. During the secondary spread, the magnitudes of these two flows change. In general, the viscous flow is dominant initially, and the capillary flow prevails at the later stages of the secondary spread. Finally, if the pores at the wall boundaries are open, capillary flow becomes more significant as its flow direction is perpendicular to the principal direction of the viscous flow causing faster secondary spread induced by a larger number of open pores at the liquid phase boundary.

Results and Discussion

The primary and secondary capillary spread for the geometry as shown in Figure 1 are solved numerically using the capillary network model with dynamic boundary condition, in which, after each discrete step, the instantaneous liquid phase pressure is found and liquid flow rate at the interface is calculated. By defining the pores as open or closed at the liquid phase boundaries, three different sets of boundary conditions are exploited: only the interface pores are defined as open in the first solution, the inlet pores, together with the interface pores are defined as open in the second solution, and, all pores, including the wall pores, are set as open in the third solution. The spread is solved over a porous medium of size ($l_x \times l_y \times lz = 10$ mm $\times$ 3 mm $\times$ 45 mm) correlated to a network consisting of ($n_x \times n_y \times nz = 33 \times 10 \times 150$) pores which gives the equivalent length $l_{eq} = l_i/ni = 0.3$ mm. Typical sand values of porous medium porosity and permeability are set, $\phi = 0.40$ and $K = 10^{-12}\mathrm{m}^2$ and later related to the parameters of a regular cubic network defined by pore radius and throat radius and length, (r_p, r_t, l_t). The pore radii are prescribed from the uniform distribution from the interval ($r_{\min}$, $r_{\max}$) and heterogeneity parameter $\chi = r_{\max}/r_{\min}-1$, with throat radii correlated to the two pores' radii, $r_{t,i,j} = (r_{p,i}+r_{p,j})/2$. As a liquid phase, the water-like fluid is used with viscosity and surface tension equal to $\mu = 10^{-3}$ Pas, and $\sigma = 7 \times 10^{-2}$ Pam. The contact angle between liquid and solid phase within porous medium is set $\theta = 0$, but any angle can be used because its influence as $\cos(\theta)$ is included in the numerical solution.

The void volume of the porous medium domain is $V_{\mathrm{void}} = 540$ mm^3, and the liquid volume is set as $V_0 = 160$ mm^3. In the primary spread, $0.3V_{\mathrm{void}}$ is filled only, and the liquid secondary spread is solved implementing the first type of the boundary condition for open pores at the interface within the porous medium. The liquid distribution is shown in Figure 3 at the end of the primary spread, and for two distinct times during the secondary spread. In Figure 3, the saturations less than $s < 0.33$ are given to better visualize the low-saturated region. The liquid spreads into previously dry porous medium, and, in the same time, the unsaturated front protrudes into the previously fully saturated region of the porous medium, with two regions located on the opposite sides of the dry/wet interface at the end of the primary spread (S_{pri}). These two spreads can be seen as simultaneous liquid imbibition by small pores and liquid drainage from the large pores. There is a large difference between the two flows, where the imbibitions flow front is smooth (still, some small fingers are observed locally as imbibition progresses) as the flow is driven by invading the small pores for which the flow is stabilized by high-flow rate (high-capillary pressure) of liquid as invading phase.[21] Having the small pores uniformly distributed throughout the volume (stochastically

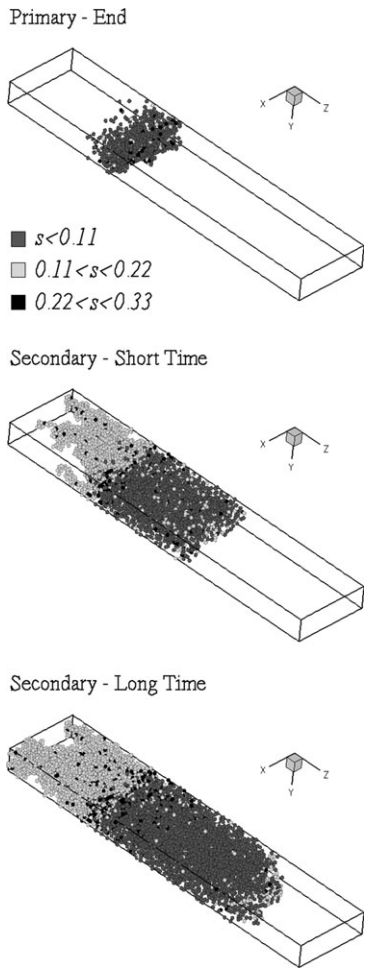

Figure 3. Secondary flow and changes of liquid distribution in porous medium in which draining (light gray) and imbibing (dark gray) subregions can be identified.

homogeneous medium), the liquid is imbibed by those pores and progresses further. Still, the flow is multiphase as only small pores are filled and large pores remain empty in this part of the porous medium. On the other hand, the drainage of large pores is slow due to the volumetric pore factor (pore volume of drained pores is larger than the pore volume of imbibing pores), and drainage instability reaches a maximum geometrical scale due to the gas phase being the invading fluid (in this study, drainage interface reaches the inlet boundary). Further drainage occurs in the remaining highly saturated regions of the porous medium.

For the second set of boundary conditions in which the inlet pores are defined as open, the secondary spread liquid distribution in draining part of the porous medium is changed compared to the previous flow case. Defining the pores at the inlet boundary as open pores, there is a liquid loss at the inlet boundary together with a protruding drainage front initiated from the S_{pri}. Two drainage fronts (from inlet and S_{pri}) are more stable as can be observed from Figure 4 but still with the principal flow direction along z-axis. On the other hand, the imbibing part of the domain remains stable (local limited fingering is observed), and again with the multiphase flow pattern. This may be attributed to the boundary type conditions and open inlet pores, where now not only does that drainage part shrink in size (interface), but there is a net flow from the inlet to the interface boundary, with the liquid transport into the imbibing part of the porous medium volume being very similar to the interface boundary conditions flow (see Figure 3 for secondary flow and short time). The evidence for different flow stability can be found from the third set of boundary conditions, in which wall pores are also defined as open. Regardless of the changes of the dominant geometrical scale in the drainage part (now in y-direction), one observes again a smooth front for the liquid flow in the imbibition part. Flow in the drainage part changes dramatically, where the liquid depletion is uniform from the overall drainage part of the domain. Clearly, such liquid distribution is a consequence of the capillary flow extent, where now, due to the large number of open pores, the liquid drains more easily from the highly saturated region.

From the numerical solution of how the liquid distribution within porous medium changes in time, the axial saturation profiles for the secondary spread are determined. Each point along the axial saturation profile is computed as an average saturation in the domain segment as shown in Figure 5. Dividing the domain in $n_d = 15$ with $n_{seg} = n_z/n_d = 10$ pores in segment z direction, the segment in Figure 5 consists of $n_x \times n_y \times n_{seg} = 33 \times 10 \times 10$ pores. The pore saturations (s_p) are depicted in one-third increments from zero

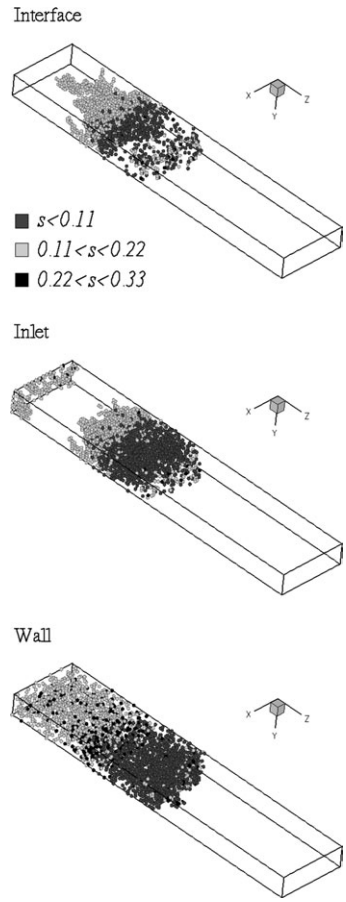

Figure 4. Variations in liquid distribution for three distinct types of the boundary conditions referred to as interface, inlet and wall types.

The liquid distribution is also influenced by geometrical dimensions which can be observed for wall boundary conditions.

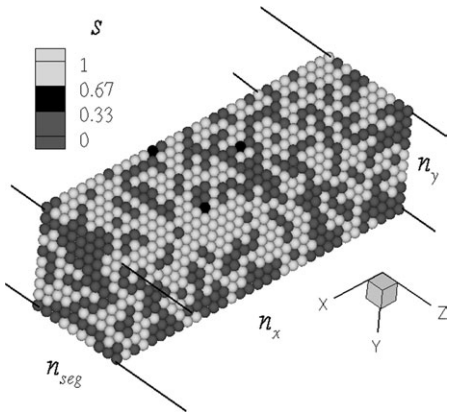

Figure 5. Averaging element defined as segment consisting of $n_x \times n_y \times n_{seg}$ pores used to calculate the saturation and flow parameters.

All quantities are assumed constant over the segment.

to one, with dark gray, black, and light gray, respectively. The segment average saturation (s) is found as a ratio of the liquid volume in segment to the segment void volume, where the liquid volume in the segment is calculated by adding the liquid volumes in each pore $s_{p,i}V_{p,i}$, and the void volume of the segment is equal to the sum of the volumes of all the pores in the segment $V_{p,i}$. Thus, calculated axial saturation profiles for all three different types of the boundary conditions are given in Figure 6, where, in each frame, the different symbols connected with lines represent saturation profiles calculated for different times throughout the secondary flow. For open pores only located at the interface, the flow backbone (continuous liquid-phase flow pattern) consists of the smallest pores. The flow backbone advances in time, but its structure does not change in the previously wetted region within the imbibition part as suggested from the axial saturation profiles. The saturation in the draining part of porous medium decreases gradually. The same saturation profiles are observed for the inlet type boundary conditions in the imbibition part, whereas the saturation in the draining part shows a maximum due to the flow at the inlet boundary. The maximum position is closer to the inlet than to the interface due to the larger number of open pores at the interface. Thus, the drainage flow rate is faster from the interface than the inlet side of the draining region. Once the wall pores are defined as open, the liquid distribution in both the imbibition and drainage parts is significantly different. In the imbibition part, the form of the flow backbone changes throughout the secondary flow, where over time, one observes some drainage in the imbibing part of the porous medium for longer times. In the draining part, the saturation profiles remain constant. Both liquid behaviors can be attributed to the decrease in the geometrical scale and an increase of the capillary flow contribution in overall liquid distribution.

As expected, a difference in the boundary conditions produces different liquid distribution in the porous medium. On the other hand, it is important to check whether the capillary pressure (p_c), and relative permeability (k_r) change with the boundary conditions. Similar to the calculation of the saturation, these two parameters are calculated over a segment, and in order to obtain how they change with saturation, they are correlated to the segment saturation obtaining $p_c(s)$ and $k_r(s)$. In previous considerations, we define the draining part of the porous medium that coincides to the wetted volume of the porous medium in the primary spread, and the imbibition part as a newly wetted region of the porous medium during the secondary flow. However, in both parts, the pores that are filled and emptied are observed. The evidence for such behavior is found from the numerical calculation, best visible for a decrease in axial saturation profiles in the imbibition part of the porous medium for wall boundary conditions. Hence, in each segment, the averaged positive and negative capillary pressure p_{cl+} and p_{cl-} (positive and negative with respect to sign of q_s), and flow rates, q_{sl+} and q_{sl-}, of all filling and all emptying pores can be distinguished as intrinsic flow properties.[22] The segment-apparent capillary pressure (p_c) is calculated as an average capillary pressure of all partially saturated pores regardless of each pore flow rate. For the overall domain, the overall flow rate of liquid is equal to zero (constant liquid

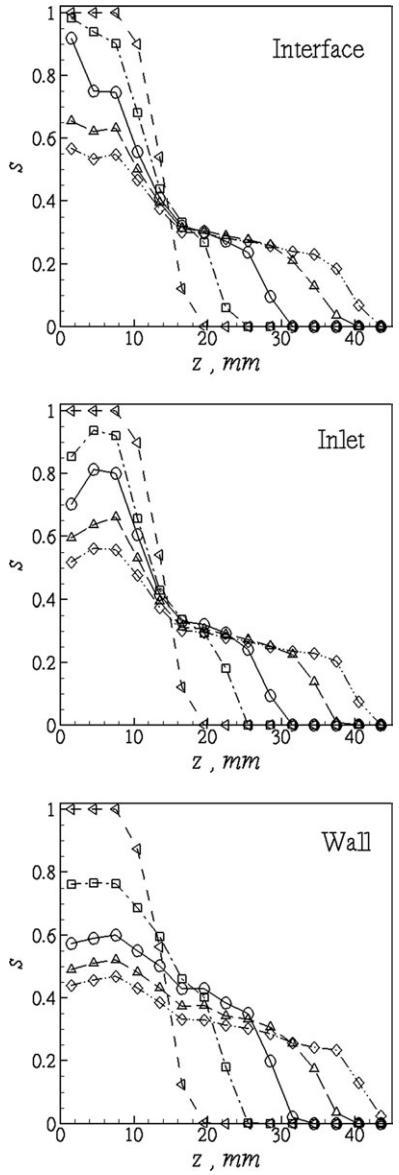

Figure 6. Axial saturation profiles $s(z)$ for three distinct boundary conditions types.

Due to the influence of open pores position and domain geometrical dimensions, the saturation profiles vary significantly. In all three frames, each saturation profile corresponds to a different secondary flow time.

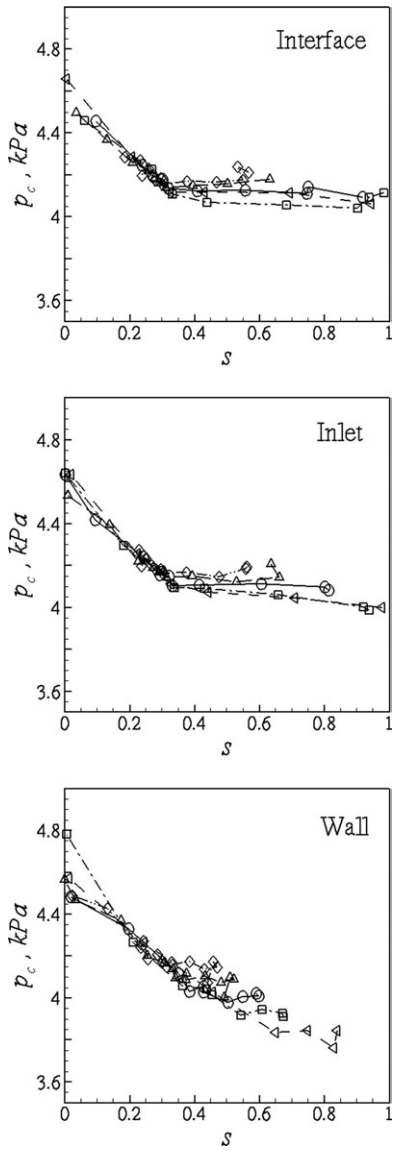

Figure 7. Changes of capillary pressure as a function of saturation, $p_c(s)$ for distinct boundary conditions.

The function $p_c(s)$ remains the same regardless of time elapsed during the secondary flow.

volume), and, for a sufficiently large segment, $q_{sl+}+q_{sl-}=0$. The maximum of q_{sl+} is in the segment to which the dry/wet interface at the end of primary spread (S_{pri}) belongs, where this segment can be defined as a reflective, with the reflective flow rate defined as $q_{ref}=2\max(q_{sl+})-q_{sl+}$, in the draining part and $q_{ref}=q_{sl+}$ in the imbibition part. The reflective flow is due to the capillary pressure difference, $p_{cl+}-p_{cl-}$. Hence, liquid-phase permeability (K_{ph}), and relative permeability (k_r) are found from the following expressions

$$K_{ph}(s)=\mu\frac{q_{ref}(s)}{l_x l_y}\frac{l_{seg}}{p_{cl+}(s)-p_{cl-}(s)} \quad \text{and} \quad k_r(s)=\frac{K_{ph}(s)}{K} \tag{4}$$

where K is porous medium (single-phase) flow permeability.

The changes of capillary pressure and relative permeability as functions of saturation $p_c(s)$ and $k_r(s)$ are shown in Figures 7 and 8 for all three types of boundary conditions. In both figures, the parameters are determined for different times throughout the secondary flow as shown with different symbols connected by lines for better visibility, and it can be observed that the parameters coincide in the whole range of saturation ($0 \le s \le 1$) regardless of elapsed time. The capillary pressure changes faster for low-saturations due to its inverse proportionality to the pore radius. For higher saturations the capillary pressure is averaged over the broader range of pore radii and the influence of small pores is lessened. On the other hand, the relative permeability shows three distinct regions where abrupt changes in $k_r(s)$ are caused by large variations in the number of pores which belong to the carrying backbone for low saturation, and, due to the presence of negative flow, q_{sl-} for high saturation. For moderate saturations, $k_r(s)$ is less influenced by saturation. In order to investigate how the parameters are influenced by the boundary conditions, the results from Figures 7 and 8 for $p_c(s)$ and $k_r(s)$ are combined as shown in Figures 9 and 10 for two parameters, respectively. Different symbols

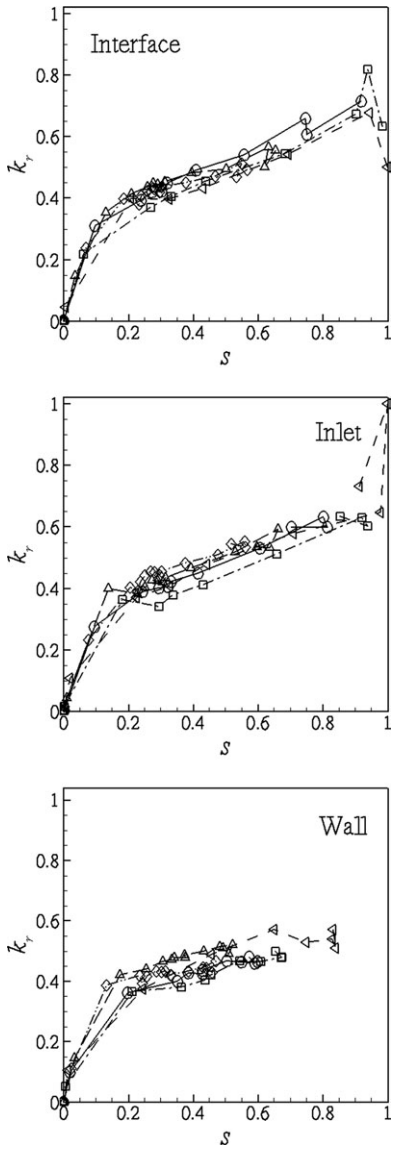

Figure 8. Change of relative permeability as a function of saturation, $k_r(s)$ for distinct boundary conditions and its invariance on the secondary flow duration.

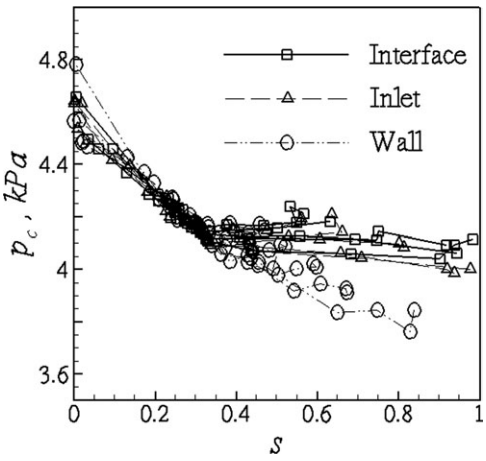

Figure 9. Invariance of capillary pressure curves $p_c(s)$ on distinct boundary conditions.

There is a slight deviation of $p_c(s)$ curves for wall boundary conditions, long time of secondary flow and high saturations (circles), but it may also be caused by the network size used in the calculations.

represent interface, inlet, and wall boundary conditions (in here, distinct times throughout the secondary flow are shown with the same symbols for each boundary conditions set), and as can be seen, numerical results suggest that $p_c(s)$ and $k_r(s)$ are the boundary conditions invariant. This is especially true for $k_r(s)$, whereas some variations of $p_c(s)$ are observed for wall boundary conditions (circles in Figure 9) which might be caused by coarse network and segment sizes used in the numerical calculations.

The numerical results reveal a few important features of the secondary capillary flow with respect to the magnitude of capillary pressure and relative permeability, invariance with respect to the flow duration time and boundary conditions, and flow stability and usage of the Darcy law to describe the fluid flow. There is a simultaneous imbibition and drainage during the secondary flow and, therefore, the capillary pressure is a weaker function of saturation compared to the primary flow. A major change in the capillary pressure is for low saturation, as the imbibition in this region is pronounced. The same arguments apply for relative permeability. As already mentioned, there are some variations in the capillary pressure and relative permeability, but both parameters still show consistent behaviors for distinct times throughout the spread and boundary conditions set (Figures 7 and 8) and, once they are compared, for different boundary conditions (Figures 9 and 10). More exclusive evidence for the invariance of two parameters could be obtained by solving the problem on the larger networks and more network random realization (we solve the problem for only one network realization). However, from the physics standpoint, the capillary pressure and relative permeability invariance for the secondary flow with distinct boundary conditions should not be mislead by capillary pressure hysteresis for the primary drainage and imbibition. In the latter case, the capillary pressure and relative permeability are compared for two different processes, imbibitions and drainage.

The results in Figures 3 and 4a show some fingering in the draining part of the porous medium (on the left hand side of the figures) for boundary conditions referred to as interface, whereas no such fingers are observed for inlet and wall boundary conditions. The fingers may be attributed to the domain size and influence of the geometrical scales, where by setting the inlet or wall boundary conditions, the magnitude of the viscous flow from Eq. 2 increases. This is especially true for the wall boundary condition, where the viscous flow length-scale is in order of medium thickness that is small in this study. For all three types of the boundary conditions, the flow front in the imbibition parts remains more stable with no pronounced capillary instability (still some fingering is observed for all three boundary conditions). As can be seen in Figures 9 and 10, the capillary pressure and relative permeability for the interface boundary conditions (squares) do not differ significantly from their inlet (triangles) and wall (circles) boundary condition counterparts. This may be explained by comparing the size of the domain and finger in Figure 3, where they are of comparable size and the single finger grows similarly to one-dimensional stable drainage flow. In this way, the draining flow is pseudo-stable. Clearly, it is of interest what would be the flow dynamics for larger domains in which more than one finger can grow simultaneously. The Darcy law and the capillary pressure and relative permeability predicted in here can be used only in a case for which the secondary capillary flow is stable as for the flow patterns observed for the inlet and wall boundary conditions. Finally, it should be noticed that besides altering the wetting characteristics of the porous media boundaries on purpose (to alter the liquid saturation in the secondary flow), different liquids in the same porous medium may behave dissimilarly, producing stable or unstable flow and corresponding saturation profiles.

Conclusions

The secondary capillary flow is formulated as a multiphase flow problem and solved numerically using the capillary network model with the potential formulation at the gas|liquid interface. Having a constant volume of liquid spreading in the porous medium and wetting previously dry regions, one observes two subregions of wetted volume behaving as mainly draining and mainly imbibition subregions. From the numerical solution, the liquid distribution

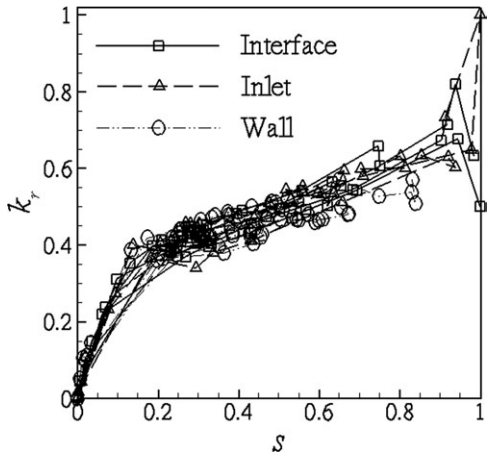

Figure 10. Comparison of relative permeability curves $k_r(s)$ for distinct boundary conditions.

There is a close agreement between all curves regardless of boundary conditions, secondary flow duration time and liquid saturation.

and flow parameters are determined for three distinct boundary conditions. These boundary conditions are obtained by varying the pore types, being *open* or *closed*, at the wetted parts of the porous medium boundaries. It is found that the liquid distribution within porous medium is greatly altered by the boundary conditions, where the averaged saturation profiles in the principal flow direction varied from gradually decreasing profiles with local maximum, to axial profiles with almost constant saturations. These saturation profiles remain self-similar in time as secondary flow progresses. From the numerical solutions, the capillary pressure and relative permeability have been determined, where it is found that both parameters are invariant with time as secondary flow progresses for a specific boundary condition, and, also, they are invariant for distinct boundary conditions. Finally, the finding that the liquid distribution in the secondary flow varies for distinct boundary conditions can be employed in applications, such as printing, baby diapers, oil recovery, by treating the porous medium boundaries (surfaces) to promote the surface pores of porous medium to behave more as open or closed pores.

Acknowledgments

We would like to thank Mr. William Ginely at the Edgewood Chemical and Biological Center (ECBC), Dr. Sari Paikoff at Defense Threat Reduction Agency (DTRA), and Mr. Joseph Kiple of KIPLE Acquisition Science and Technology for their support throughout the Agent Fate Project.

Literature Cited

1. Bear J. *Dynamics of Fluids in Porous Media*. New York: Dover Publications, Inc.; 1988.
2. Dullien FAL. *Porous Media: Fluid Transport and Pore Structure*. New York: Academic Press; 1992.
3. Piekaar HW, Clarenburg LA. Aerosol filters - pore size distribution in fibrous filters. *Chem Eng Sci*. 1967;22:1399–1408.
4. Markicevic B, Navaz HK. Primary and secondary infiltration of wetting liquid sessile droplet into porous media. *Trans Porous Media*. 2010a;85:953–974.
5. Aggelopoulos CA, Tsakiroglou CD. The effect of micro-heterogeneity and capillary number on capillary pressure and relative permeability curves of soils. *Geoderma*. 2008;148:25–34.
6. Markicevic B, Navaz, HK. The influence of capillary flow on the fate of evaporating wetted imprint of the sessile droplet in porous medium. *Phys Fluids*. 2010b;22:122103.
7. Markicevic B, D'Onofrio TG, Navaz HK. On spread extent of sessile droplet into porous medium: Numerical solution and comparisons with experiments. *Phys Fluids*. 2010;22:012103.
8. Le Bray Y, Prat M. Three-dimensional pore network simulation of drying in capillary porous media. *Int J Heat Mass Transfer*. 1999;42:4207–4224.
9. Prat M. On the influence of pore shape, contact angle and film flows on drying of capillary porous media. *Int J Heat Mass Transfer*. 2007;50:1455–1468.
10. Yiotis AG, Stubos AK, Boudouvis AG, Yortsos YC. A 2-D pore network model of the drying of single-component liquids in porous media. *Adv Water Transport*. 2001;24:439–460.
11. Yiotis AG, Tsimpanogiannis IN, Stubos AK, Yortsos YC. Pore-network study of the characteristic periods in the drying of porous materials. *J. Colloid Interface Sci*., 2006;297:738–748.
12. Fatt I. The network model of porous media III. Dynamic properties of networks with tube radius distribution. *Trans AIME*. 1956;207:164–181.
13. Wilkinson D, Willemsen JF. Invasion percolation - a new form of percolation theory. *J Phys A*. 1983;16:3365–3376.
14. Valavanides MS, Payatakes AC. True-to-mechanism model of steady-state two-phase flow in porous media, using decomposition into prototype flows. *Adv Water Resour*. 2001;24:385–407.
15. Tsakiroglou CD, Sygouni V, Aggelopoulos CA. A dynamic network-type simulator to investigare the multiphase flow properties of heterogeneous soils. *Vadose Zone J*. 2010;9:285–294.
16. Lenormand R, Touboul E, Zarcone C. Numerical models and experiments on immiscible displacement in porous media. *J Fluid Mech*. 1988;189:165–187.
17. Yortsos YC, Xu B, Salin D. Phase diagram of fully developed drainage in porous media. *Phys Rev Lett*. 1997;79:4581–4584.
18. Plourde F, Prat M. Pore network simulations of drying of capillary porous media. Influence of thermal gradients. *Int J Heat Mass Transfer*. 2003;46:1293–1307.
19. Or D. Scaling of capillary, gravity and viscous forces affecting flow morphology in unsaturated porous media. *Adv Water Transport*. 2008;31:1129–1136.
20. Markicevic B, Navaz HK. Numerical solution of wetting fluid spread into porous media. *Int J Num Meth Heat Fluid Flow*. 2009;19:521–534.
21. Meheust Y, Lovoll G, Maloy KJ, Schmittbuhl J. Interface scaling in a two-dimensional porous medium under combined viscous, gravity and capillary effects. *Phys Rev E*. 2002;66:051603.
22. Pop IS, van Duijn CJ, Niessner J, Hassanizadeh SM. Horizontal redistribution of fluids in a porous medium: The role of interfacial area in modeling hysteresis. *Adv Water Resour*. 2009;32:383–390.

Manuscript received Apr. 5, 2011, and revision received Sept. 23, 2011.